The Slit/Robo system suppresses hepatocyte growth factor-dependent invasion and morphogenesis

UNIVERSITÀ DEGLI STUDI DI TORINO

The Slit/Robo System Suppresses Hepatocyte Growth Factor-dependent Invasion and Morphogenesis

Maria Cristina Stella, Livio Trusolino, and Paolo M. Comoglio

Author Affiliations

Division of Molecular Oncology, Institute for Cancer Research and Treatment, University of Torino School of Medicine, 10060 Candiolo, Torino, Italy

Richard O. Hynes, Monitoring Editor

Submitted March 27, 2008.

Revised August 11, 2008.

Accepted November 4, 2008.

Abstract

The Slit protein acts through the Roundabout receptor as a paracrine chemorepellent in axon guidance and as an inhibitor in leukocyte chemotaxis, but its role in epithelial cell motility and morphogenesis remains largely unexplored. We report that nontransformed epithelial cells and cancerous cells empower the Slit-2/Robo1 signaling system to limit outward migration in response to motogenic attractants and to remain positionally confined within their primitive location. Short hairpin RNA-mediated depletion of SLIT-2 or ectopic expression of a soluble decoy Robo enhance hepatocyte growth factor (HGF)-induced migration, matrix invasion, and tubulogenesis, concomitantly with the up-regulation of Cdc-42 and the down-modulation of Rac-1 activities. Accordingly, autocrine overexpression or exogenous administration of Slit-2 prevent HGF-triggered motile responses, reduce Cdc-42 activation, and stimulate Rac-1. This antimigratory activity of Slit-2 derives from the inhibition of actin-based protrusive forces and from an increased adhesive strength of cadherin-mediated intercellular contacts. These results disclose a novel function for Slit and Robo in the inhibition of growth factor-mediated epithelial cell motility and morphogenesis, invoking a critical role for both molecules as natural antagonists of neoplastic invasive growth.

1. Introduction

Morphogenetic events, such as formation of branched tubular structures, angiogenesis, and neuronal networking, are modulated by a number of soluble and immobilized molecules that act as either attractants or repellents, including growth factors, extracellular matrix components, proteases, and morphogens (Lecuit and Lenne, 2007). There is now increasing evidence that cancer cells hijack the strategies by which the embryo grows and develops and that invading tumors coopt the genetic and signaling mechanisms underlying tissue morphogenesis for the proper execution of neoplastic dissemination (Huber et al., 2005). Therefore, insight into developmental programs is likely to illuminate essential aspects of cancer progression.

Slit, acting through the transmembrane receptor Roundabout (Robo), belongs to a recently identified family of secreted repellents (Wong et al., 2002). Despite the considerable body of knowledge gathered so far on the function of Slit and Robo in axon guidance (Dickson and Gilestro, 2006), neuronal migration (Wu et al., 1999), leukocyte chemotaxis (Wu et al., 2001) and angiogenesis (Wang et al., 2003), the information on the effects of the Slit/Robo system in normal and neoplastic epithelial cells is still fragmentary. If there is a general conservation of guidance mechanisms underlying cell migration and morphogenesis in different cell types, then Slit should limit the locomotion of Robo-expressing epithelial cells toward attractive stimuli. More importantly, it should sidetrack invading carcinomas away from attractants produced in the microenvironment.

In this article, we sought to explore this issue using hepatocyte growth factor (HGF) as an attractive cue. HGF and its tyrosine kinase receptor Met play a crucial role both in development and cancer (Comoglio and Trusolino, 2002). During organogenesis HGF acts as a motogen and morphogen and stimulates, among other things, the directional migration of myoblasts from the somites to the limbs as well as the guidance of motoneurons toward striated muscles (Birchmeier and Gherardi, 1998; Maina and Klein, 1999). In neoplastic contexts, activation of Met correlates with a metastatic phenotype and a poor prognosis in several carcinomas, and HGF stromal gradients favor tumor dissemination (Birchmeier et al., 2003).

We show here that immortalized, nontransformed epithelial cells as well as carcinoma and melanoma cells frequently display a Slit/Robo signaling that endogenously counteracts HGF-driven migration, invasion, and morphogenesis. Mechanistically, this Slit-dependent inhibitory activity resides in the reinforcement of the intercellular junctional apparatus (which impairs cell–cell dissociation) and in the weakening of protrusive forces (which decreases cell motility), possibly as a consequence of concomitant up-regulation of Rac-1 and down-regulation of Cdc-42 activities. Together, these results point to a fundamental role for Slit and Robo as anti-invasive cues during epithelial morphogenesis and neoplastic progression.

2. MATERIALS AND METHODS

Endpoint Polymerase Chain Reaction (PCR) and Primers

ROBO-N and SLIT-2-Myc cDNAs were obtained by direct amplification of MDA-MB-435–retrotranscribed mRNAs. The primers used were the following: 5'-ACT ATA TAT AGT ATT AAA CTA TTA ACT CTA GAA TGA AAT GGA AAC ATG TTC CTT TTT TGG-3' (sense Robo-N) and 5'-AAC TAA ATG TAA TAC TAA TTT ATT AAA CGC GTT TAA GCG TAA TCT GGA ACA TCA TAT GGG TAG TTG GCT CCA GAT GGC CGA TAG AGA ATT TTA TAT CCT TGT ATA TAC-3' (antisense ROBO-N, HA-tagged); 5'-ACC TTA GAC ATG CGC GGC GTT GGC TGG CAG ATG CTG TCC CTG-3' (sense Slit-2); 5'-TAT TAA TCT AGA TTA ATT CAG ATC CTC TTC TGA GAT GAG TTT TTG TTC GGA CAC ACA CCT CGT ACA GCC GC-3' (antisense Slit-2, Myc-tagged). Both ROBO-N-HA and SLIT-2-Myc were cloned by blunt-end ligation in the retroviral vector pLHCX (Clontech, Mountain View, CA). The sequences of the two SLIT-2-shRNAs, derived from a screening performed using the SUPER RNA interference (RNAi) library (Brummelkamp et al., 2002) were the following: 5'-GAA CGT GTC CCG ATT AGA G-3' (sequence A) and 5'-CTG CCT TCG GGT AGA TGC T-3' (sequence b); the scrambled, control short hairpin RNA (shRNA) used in MDA-MB-435 cells was GAA GGT GGG GTA GAT GCT A; sequence B was used for silencing SLIT-2 expression in Madin-Darby canine kidney (MDCK) cells as well, whereas in this cell line sequence A, which does not target canine SLIT-2, was used as a control. The sequences of the three Robo-1 shRNA, derived from the specific MISSION shRNA Gene Family Sets (Sigma-Aldrich, St. Louis, MO) were 5'-AGA AAT ACA GTC ACA TTA TCT C-3' (sequence A); 5'-CCA CCA TTT CAT GGA AGA ACT C-3' (sequence B); 5'-CAC CAG CAA GGA TGT ATT TCT C-3' (sequence C). Sequence C was used for silencing Robo-1 in MDCK cells. Scramble MISSION shRNAs were provided by Sigma-Aldrich. The primers used for endpoint PCRs in human-derived cell lines were 5'-TGC CGC AAG CTC TAC TGC CTG-3' (sense Slit-1); 5'-GCA CTG GCA GCT GTA GGA AAG A-3' (antisense Slit-1); 5'-GCA TTT TGC CTG GCT GTG AG-3' (sense Slit-2); 5'-CAT TGA TGG GCA AGC AGG TG-3' (antisense Slit-2); 5'-TGG AGA AGG ACA GCG TGG TG3' (sense Slit-3); 5'-GAG CAG GCA TTG GCA GAG TC-3' (antisense Slit-3); 5'-CCT CGC ATT GTT GAA CAC C-3' (sense Robo-1); 5'-AAC ATT CGG TGT GAG CGA GG-3' (antisense Robo-1); 5'-AAG CTC TCT AGA GAG ACA AC-3' (sense Robo-2); 5'-TGG GCT TGC TAT AGG GCA CC-3' (antisense Robo-2); 5'-GGT CAC CCC ATC CCG AAG GG-3' (sense Robo-3); 5'-CAC CCA AGC CAG CAG GCC T-3' (antisense Robo-3); 5'-GCT GGC CCA GCT CTC CAG CC-3' (sense Robo-4); and 5'-ACT CAC AGG CCC GGA GCT CC-3' (antisense Robo-4). The primers used for MDCK cell amplifications were 5'-TGC CGA AAG CTC TAC TGC CTG-3' (sense Slit-1); 5'-GCA CTG GCA GCT GTA GGA AAG-3' (antisense Slit-1); 5'-GCA TTT TGC CTG GCT GTG AG-3' (sense Slit-2); 5'-CGT TGA TGG GCA AGC AGG TG-3' (antisense Slit-2); 5'-CCA GCA GTA GGC ATC AAC AGC-3' (sense Slit-3); 5'-CAC CAC GCT GTC CTT CTC CA-3' (antisense Slit-3); 5'-ATG AGC AAT TTA GAG AAA TGT GG-3' (sense Robo-1); 5'-ggc gtg ggg cgg cct tca gct t-3' (antisense Robo-1); 5'-CCA GAC CCC TGA GAG CAC TA-3' (sense Robo-2); 5'-TGG GCT TGC TGT ATG GCA CC-3' (antisense Robo-2); 5'-CTT GGG ATG GAG GGA CCA AGC-3'

(sense Robo-3); 5'-CAC CCA CGC CAG CAG GCC T-3' (antisense Robo-3); 5'-GCT GGC CCG GCT CTC CAG CC-3' (sense Robo-4); and 5'-GGG AAA GGT TCT TGG AGC CTC T-3' (antisense Robo-4). Primers for semiquantitative real-time PCR were the following: for Slit-2, designed in two contiguous exons, 5'-GCA TTT TGC CTG GCT GTG AG-3' (sense Slit-2, MDA-MB-435); 5'-CAT TGA TGG GCA AGC AGG TG-3' (antisense Slit-2, MDA-MB-435); 5'-GCA TTT TGC CTG GCT GTG AG-3' (sense Slit-2, MDCK); and 5'-CGT TGA TGG GCA AGC AGG TG-3' (antisense Slit-2, MDCK). The housekeeping gene phospho-glycerate-kinase (PGK) was chosen as a standard reference. The primers were 5'-CTT ATG AGC CAC CTA GGC CG-3' (sense PGK, MDA-MB-435); 5'-CAT CCT TGC CCA GCA GAG AT-3' (antisense PGK, MDA-MB-435); 5'-ATC ACA GGT GGT GGA GAC AC-3' (sense PGK, MDCK); and 5'-CTA ATG CCA ACC AGA GAT AG-3' (antisense PGK, MDCK). Total RNAs were obtained using the RNeasy Mini kit (QIAGEN, Valencia, CA) and quantified using RNA Nano Chips (Agilent Technologies, Santa Clara, CA) together with a 2100 Bioanalyzer (Agilent Technologies). cDNAs were retro-transcribed with High Capacity cDNA Reverse Transcription kit (Applied Biosystems, Foster City, CA). PCR amplifications were monitored using a 7009 HT Analyzer (Applied Biosystems) under the following thermocycler conditions: stage 1, 95°C for 10 min for one cycle; and stage 2, 95°C for 15 s and 64°C for 1 min for 60 cycles.

Antibodies

We used the following antibodies: anti-actin, anti-hemagglutinin (HA), biotin-conjugated anti-Myc (Santa Cruz Biotechnology, Santa Cruz, CA); anti-Rac 1, anti-Cdc42, anti-E-cadherin, and anti-β-catenin (BD Biosciences, San Jose, CA); anti-Myc (clone 9E10; Millipore, Billerica, MA); anti-vinculin and anti-FLAG (Sigma-Aldrich); and anti-Cdc-42 (Santa Cruz Biotechnology). The anti-zona occludens (ZO)-1 monoclonal antibody (mAb), developed by D. Goodenough, was obtained from the Developmental Studies Hybridoma Bank (University of Iowa, Iowa City, IA).

Cell Culture and Viral Infection

MDA-MB-435, MDCK, U-87, RKO, HT-29, 769-P, and COS-7 were cultured in DMEM; Skov-3, DLD-1, HCT-116, and N-87 were cultured in RPMI 1640 medium; LoVo was cultured in Ham's F-12; Hec-1A and RT-112 were cultured in McCoy's 5A; and HeLa was cultured in Iscove. All media were supplemented with 10% FCS (Sigma). Expression of exogenous proteins was obtained with LipofectAMINE 2000 (Invitrogen)-mediated transfection or with viral infection. MISSION shRNA lentiviral particles were prepared according to the instruction of the manufacturer. Human cells were infected with a multiplicity of infection (MOI) of 30, whereas canine MDCK cells were infected with an MOI of 90. Retroviral hybrid vectors were produced by transient transfection of 293T cells. Viral supernatants were filtered through a 0.22-μm filter, and infections were performed in the presence of 4 μg/ml Polybrene (Sigma-Aldrich), followed by selection with puromycin (Sigma-Aldrich) or hygromycin-B (Invitrogen).

Biochemistry

The expression of Rac-1-gof-Myc, Rac-1-DN-Myc, Cdc42-DN-HA, Cdc-42-gof-FLAG, and Slit-2-Myc was analyzed by immunoprecipitation. For immunoprecipitations, 5 × 106 cells were lysed for 20 min at 4°C with 1 ml of a buffer containing 50 mM HEPES, pH 7.4, 5 mM EDTA, 2 mM EGTA, 150 mM NaCl, 10% glycerol, and 1% Triton X-100, in the presence of protease and phosphatase inhibitors. Extracts were clarified at 12,000 rpm for 15 min, normalized with the BCA Protein Assay Reagent kit (Pierce Chemical, Rockford, IL), and incubated with different mAbs for 2 h at 4°C. Immune complexes were collected with either protein G- or protein A-Sepharose, washed in lysis buffer, and eluted. Total cellular proteins were extracted by solubilizing the cells in boiling SDS buffer (50 mM Tris-HCl, pH 7.5, 150 mM NaCl, and 1% SDS). Extracts were electrophoresed on SDS-polyacrylamide gels and transferred onto nitrocellulose membranes (Hybond; GE Healthcare, Little Chalfont, Buckinghamshire, United Kingdom). Nitrocellulose-bound antibodies were detected by the enhanced chemiluminescence system (GE Healthcare). Western blot analyses to detect E-cadherin were performed using protein extracts derived from 6 × 104 MDCK cells suspended as hanging drops (see below). Pool-down experiments were done using PAK-GST protein beads (Cytoskeleton, Denver, CO), and 80% confluent cells starved for 24 h (Sander et al., 1998). For Cdc-42 pool-down experiments, 50 μg of PAK-GST proteins

were incubated with 10 mg of whole cell lysates; for Rac-1, 20 μg of PAK-GST proteins were incubated with 2 mg of whole cell lysates.

Biological Assays

In all the biological assays, we used baculovirus-derived recombinant HGF (Naldini et al., 1995). If not otherwise indicated, HGF was used at a concentration of 25 ng/ml for the migration assays and at a concentration of 100 ng/ml for tubulogenesis. Slit-2-Myc–tagged protein was obtained from the supernatant of Chinese hamster ovary (CHO) cells retrovirally infected with Slit-2-Myc, grown in serum-free medium. Because Slit-2 is frequently associated to heparan sulfate glycosaminoglycans (Liang et al., 1999; Ronca et al., 2001), the production and release of Slit-2 were optimized using CHO cells defective in proteoglycan synthesis (Esko et al., 1987). Conditioned medium was concentrated using Centricon Plus-20 (Millipore) centrifugal filter devices, with a cut-off of 100 kDa. The amount of Slit-2-Myc in each preparation was quantified by silver staining. Eighty nanograms of concentrated Slit2-Myc polypeptide were used in combination with 20 ng of HGF. Always, soluble Slit 2-Myc polypeptide was administrated together with heparin, as described previously (Hussain et al., 2006). Transwell migration and tubulogenesis assays were performed and quantified as described previously (Stella et al., 2005). Images were captured every with ImageReady software (Adobe Systems, Mountain View, CA) and arranged using Photoshop software (Adobe Systems). Scratch assays were performed as described previously (Michieli et al., 2004) and quantified by time-lapse microscopy (1 image every 10 min), plotting the distance between the scratch margins measured as mean of 10 different measurements expressed as percentage of the initial distance. Aggregation assays were performed as described previously (Thoreson et al., 2000). After 12 h, aggregates were counted and stained with trypan blue to monitor cell viability. Images were recorded as specified above. For motility assays in the presence of an HGF isotropic gradient, cells were plated onto 24 multiwell culture plates (MatTek, Ashland, MA), maintained in DMEM lacking phenol red (Sigma-Aldrich). Video images were recorded at 10-min intervals for 36 h; images were analyzed and arranged using Sony Vegas software (Sony Media Software, Tokyo, Japan) in combination with Microsoft Office Excel (Microsoft, Redmond, WA).

Immunofluorescence

Cells were seeded onto gelatin-coated glass coverslips. At the indicated times, cells were fixed, permeabilized, and blocked in 10% fetal calf serum (FCS). Primary antibodies were incubated for 12 h at 4°C followed by staining with fluorochrome-conjugated secondary antibodies (Invitrogen, Carlsbad, CA). F-actin was evidenced with tetramethylrhodamine B isothiocyanate (TRITC)-conjugated phalloidin. The stained cells were mounted in Mowiol and observed and photographed using a confocal laser scanning system.

Statistical and Densitometric Analysis

Results are means ± SD or SEM. Comparisons were made using the two-tailed Student's t test. p values <0.05 were considered to be statistically significant. In each experimental point were scored 10 cells for isotropic migration assays and 100 cysts together with 100 tubules for tubulogenesis analysis. Blot images were captured using a ChemiDoc XRS molecular imager (Bio-Rad, Hercules, CA). Densitometric analysis was performed with a Quantity One one-dimensional analysis software installed on the imager.

3. RESULTS

Inhibition of Slit-2 or Robo-1 in Melanoma Cells Enhances HGF-mediated Motility and Invasion

There are three Slits and four Robos in mammals (Wong et al., 2002). Evidences from the literature indicate that Slit-2, among all the Slit ligands, is the isoform most frequently expressed in melanomas and carcinomas (Wang et al., 2003). We decided to integrate this analysis by exploring, in parallel with Slit-2, Robo-1 expression in human cell lines. Reverse transcription (RT)-PCR analysis in 14 tumor cell lines derived from various tissues revealed that five lines (Skov-3, HeLa, MDA-MB-435, 769-P, and Hec-1A) displayed basal expression of both ROBO-1 and SLIT-2 genes (Table 1). Detailed investigation of the full panel of SLIT and ROBO transcripts in these five cell lines indicated that, in addition to Slit-2 and

Robo-1, HeLa, 769-P, and Hec-1A cells express Slit-1, Slit-3, and Robo-3; Skov-3 express Slit-3 and Robo-3; and finally, MDA-MB-435 cells express two Robo receptors, Robo-1 and Robo-3, but only one Slit gene, Slit-2 (Figure 1A)

Figure 1. Slit-2 down-regulation enhances HGF-dependent motogenesis and morphogenesis in MDA-MB-435 cells. (A) Endpoint RT-PCR expression of SLIT and ROBO genes; (−): PCR reaction performed without template. (B) Variations of SLIT-2 mRNA in MDA-MB-435 cells in the following experimental conditions: wild-type cells (−); cells transduced with a scrambled shRNA sequence (ctr); cells transduced with two different SLIT-2-specific shRNAs (A and B); cells cotransduced with shRNA B together with a Myc-tagged variant of SLIT-2. Transcript quantitations are shown as –fold variations of SLIT-2 mRNA content with respect to wild-type cells. Data are the means ± SD (error bars) of four independent experiments, performed in triplicate. (C) Time course analysis of the HGF-dependent anisotropic migration (transwell assay) in cells expressing a scrambled shRNA (−), the SLIT-2 shRNA B (+), or coexpressing the SLIT-2 shRNA B together with Slit-2-Myc. Data are the means ± SD (error bars) of five independent experiments, performed in duplicate. *$p < 0.05$ at 6 h and **$p < 0.01$ at 12 h. (D) Migratory trajectories of cells expressing either a scrambled shRNA (−) or the SLIT-2 shRNA B (+) in the absence (−) or presence (+) of HGF. Images were recorded every 10 min for 36 h by time-lapse videomicroscopy. The diagram shows the trajectories of two representative cells for each experimental condition. The lower panel quantitates the total distance covered in 36 h. The average values ± SEM, expressed in micrometers, derive from analysis of 10 cells for each experimental condition. This experiment was repeated three times in duplicate. (E) Collagen invasion (tubulogenesis) assay in MDA-MB-435 cells expressing the scrambled (−) or the SLIT-2 shRNA B (+). Cells were treated with vehicle (−) or with HGF (+). The micrographs show representative 4-d-old colonies. Bar, 20 μm. The bottom panel corresponds to the morphometric analysis of the collagen invasion assay presented in the top panel. The average number of sprouting cells in each cyst and the average length of single tubules together ± SEM are shown.

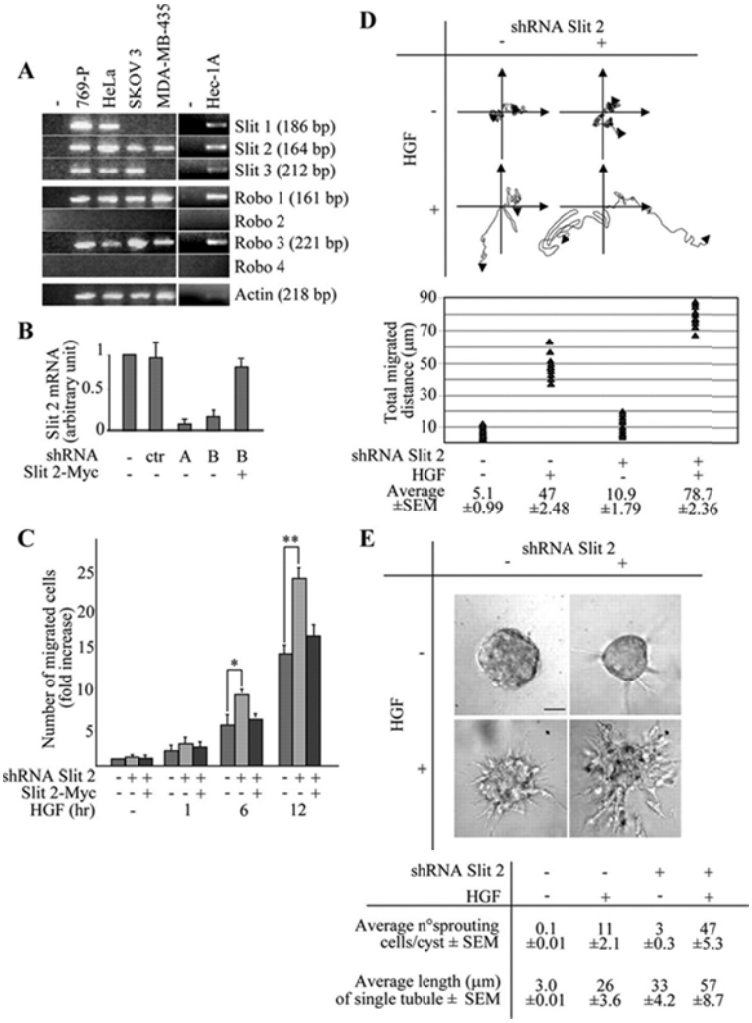

We started our experiments by abrogating Slit-2 function in MDA-MB-435, a melanoma cell line that has been extensively characterized in terms of motile and invasive responses upon stimulation with motogenic cytokines, such as HGF (Trusolino et al., 2001; Michieli et al., 2004; Stella et al., 2005). Moreover, these cells have the unique property of expressing Slit-2 as the sole member of this ligand family, which alleviates concerns of redundancy and therefore facilitates initial biological investigation. To inhibit Slit-2 expression, we used two short hairpin RNAs (shRNA-A and shRNA-B; see Supplemental Material) that abated the expression of the SLIT-2 gene by 80–90%, as assessed by quantitative real time RT-PCR (Figure 1B). A scrambled shRNA was used as a control in all the experiments (Figure 1B). Analysis of HGF-dependent cell motility in cells with normal or diminished levels of Slit-2 was performed using several in vitro assays meant to assess different parameters, including directional migration across transwell-permeable filters toward a polarized source of ligand (anisotropic conditions), random migration on plastic dishes (isotropic conditions), and matrix invasion in three-dimensional cultures. Time course analyses of anisotropic cell migration revealed that Slit-2–deficient cells displayed an enhanced chemotactic response to HGF in a time-dependent manner (Figure 1C). The rescue of Slit-2 expression through retroviral transduction of a Myc-tagged variant of Slit-2 restored HGF-dependent cell migration at levels comparable with those observed in control cells (Figure 1, B and C). In isotropic conditions, cells lacking Slit-2 as well as control cells exhibited a highly variable motogenic behavior, moving around with frequent changes of direction, in a somewhat erratic manner. However, Slit-2–deficient cells were characterized by a statistically significant increase in the total traveled distance (Figure 1D). Finally, in a three-dimensional collagen invasion assay (tubulogenesis assay), cells with impaired expression of Slit-2 were able to invade collagen much more efficiently than control cells upon treatment with HGF (Figure 1E). Slit-2 silencing resulted in a modest, but clearly detectable, tubulogenic activity also under basal conditions, in the absence of exogenous HGF (Figure 1E). This suggests that the Slit/Robo circuit chronically operative in these cells conveys constitutive repelling signals that prevent cells from moving toward attractive stimuli present in the adjacent matrix. As a complementary approach to inhibit Slit-2 function, we transduced MDA-MB-435 cells with an HA-tagged variant of Robo-N, a fragment of Robo-1 that contains only the extracellular part of the Robo protein and acts as a dominant-interfering decoy receptor (Wu et al., 1999) (Figure 2A). When subjected to a transwell migration assay (Figure 2B) or to a collagen invasion assay (Figure 2C) in the presence of HGF, cells expressing Robo-N were more efficient than control cells.

Figure 2. A dominant-negative form of Robo receptor (Robo-N) as well as Robo-1 down-regulation stimulate HGF-dependent cell migration and tubulogenesis in MDA-MB-435 cells. (A) Anti-HA Western blot expression of Robo-N-HA in MDA-MB-435 cells. Actin is shown as a control for protein loading. (B) Anisotropic migration of MDA-MB-435 cells expressing Robo-N after 12 h of HGF treatment. Data are the means ± SD (error bars) of three independent experiments performed in duplicate. **$p < 0.01$. (C) Tubulogenesis assay in control (−) and Robo-N (+) cells. Cells were treated with vehicle (−) or with HGF (+) for 4 d. Bar, 20 μm. Morphometric analysis is presented in the bottom panel. (D) Variations of ROBO-1 mRNA in MDA-MB-435 cells in the following experimental conditions: wild-type cells (−); cells transduced with a scrambled shRNA sequence (ctr); cells transduced with three different ROBO-1–specific shRNAs (A–C). Transcript quantitations are shown as -fold variations of ROBO-1 mRNA content with respect to wild-type cells. Data are the means ± SD (error bars) of two independent experiments, performed in triplicate. (E) Anisotropic migration (transwell assay) in cells expressing a scrambled shRNA (−) or the ROBO-1 shRNA B (+) after 12 h of HGF treatment. Data are the means ± SD (error bars) of three independent experiments, performed in duplicate. **$p < 0.01$. (F) Tubulogenesis assay in MDA-MB-435 cells expressing the scrambled (−) or the ROBO-1 (+) shRNA B. Cells were treated with vehicle (−) or with HGF (+). The micrographs show representative four-day old colonies. Bar, 20 μm. The lower panel corresponds to the morphometric analysis of the collagen invasion assay presented in the top panel. The average number of sprouting cells in each cyst and the average length of single tubules together ± SEM are shown.

Finally, we validated these findings by inhibiting Robo-1 instead of Slit-2. Indeed, reduction of Robo-1 by shRNA technology (Figure 2D) sensitized cells to HGF in both anisotropic cell migration (Figure 2E) and collagen invasion (Figure 2F). Together, these results indicate that genetic attenuation of the Slit/Robo pathway—through either silencing of the ligand, silencing of the receptor, or overexpression of a dominant negative isoform of the receptor—exacerbates the HGF-dependent motile and invasive properties of neoplastic cells.

Hyperactivation of the Slit/Robo Pathway in Melanoma Cells Suppresses HGF-dependent Responses

In parallel with inhibition of the Slit/Robo system, we attempted a gain-of-function approach by enhancing Slit/Robo signaling using three different experimental conditions: 1) potentiation of the endogenous loop by ectopic overexpression of the SLIT-2 gene, 2) exogenous administration of the recombinant Slit-2 protein, and 3) coculture experiments using human embryonic kidney (HEK) cells stably producing Slit-2. In the first setting (Figure 3A), Slit-2 overexpression substantially impaired the chemotactic responsiveness to HGF in transwell assays, which was restored upon shRNA-mediated down-modulation of Slit-2 itself (Figure 3, A and B). Under isotropic condition, Slit-2-overexpressing cells displayed a static, nonmotile phenotype and were completely insensitive to HGF treatment (data not shown). Similarly, in a collagen invasion assay, the tubulogenic response to HGF was much weaker in Slit-2–overexpressing cells than in control cells (Figure 3C).

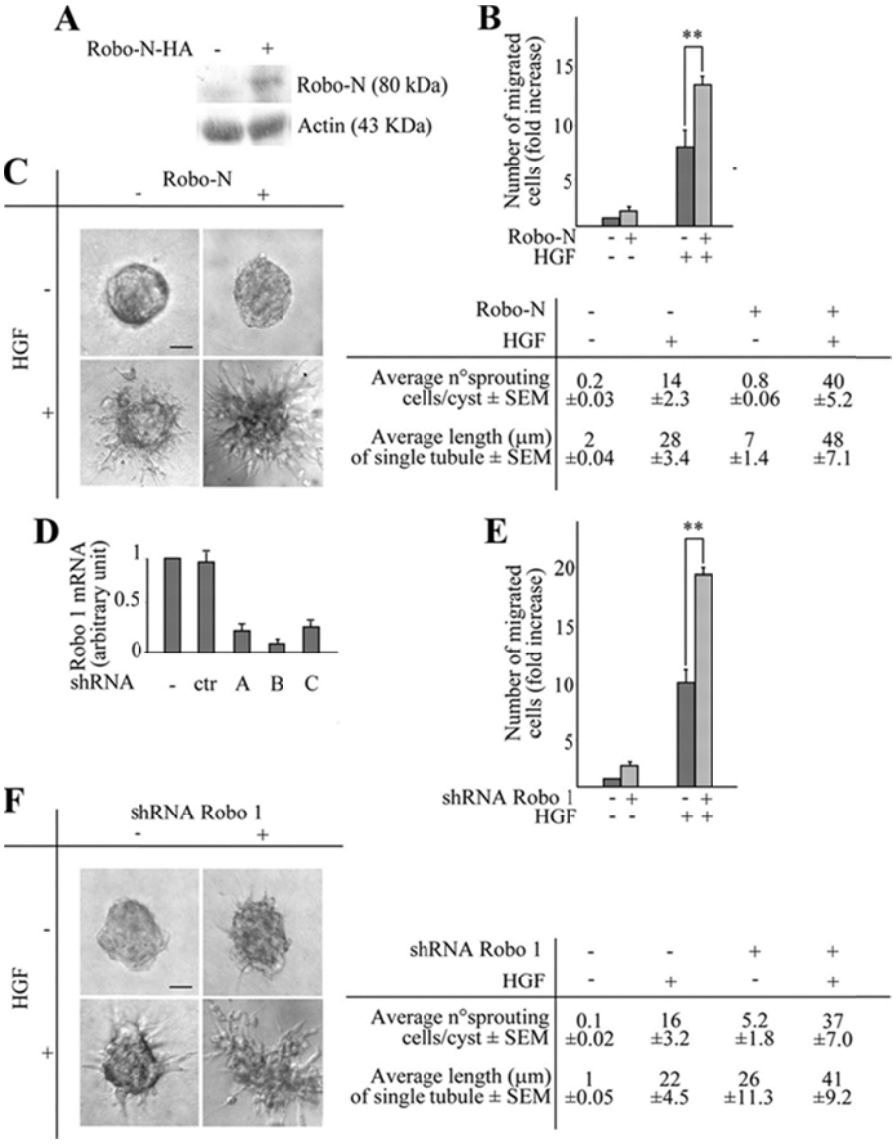

Figure 3. Slit-2 inhibits HGF-dependent cell migration and tubulogenesis in MDA-MB-435 cells. (A) Anti-Myc Western blot expression of Slit-2-Myc in MDA-MB-435 cells. Cotransduction with the SLIT-2-specific shRNA B abrogates the expression of Slit-2-Myc. (B) HGF-dependent anisotropic migration in cells transduced with an empty vector, a Slit-2-Myc vector, or cotransduced with Slit-2-Myc together with the SLIT-2-specific shRNA-B. Cells were either left untreated or stimulated with HGF for 12 h. Data are the means ± SD (error bars) of three independent experiments performed in duplicate. **$p < 0.01$ at 12 h. (C) Tubulogenesis assay in cells expressing the empty (−) or the Slit-2-Myc (+) vector, in the presence of vehicle (−) or HGF (+). The micrographs show representative 10-d old colonies. Bar, 20 µm.

Morphometric analysis is in the bottom panel. (D) Anti-Myc Western blot of conditioned media obtained from CHO cells infected with a control empty virus (−) or with a virus encoding for Slit-2-Myc (+). Immunodepletion of Slit-2 from the culture supernatants using anti-Myc antibodies is also shown. (E) Anisotropic migration of MDA-MB-435 cells in the presence of control supernatant, Slit-2–containing supernatant, or Slit-2–depleted supernatant. This analysis was performed after 12 h of HGF treatment. Data are the means ± SD (error bars) of three independent experiments performed in duplicate. ***$p < 0.001$. (F) Tubulogenesis assay in MDA-MB-435 cells in the presence of Slit-2–immunodepleted (−) or Slit-2–containing (+) medium, with or without HGF. The micrographs show representative 4-d-old colonies. Bar, 20 µm. Morphometric analysis is in the bottom panel. (G) Western blot expression of Slit 2-Myc in HEK cells. (H) Anisotropic migration of MDA-MB-435 cells cocultured with HEK cells expressing or not expressing Slit-2-Myc. Cell migration was quantitated after 12 h of HGF treatment. Data are the means ± SD (error bars) of two independent experiments performed in duplicate. **$p < 0.01$. (I) Anisotropic migration of MDA-MB-435 cells expressing a scrambled shRNA (−) or the ROBO-1–specific shRNA B (+) in the presence of Slit-2–containing (+) or Slit-2–depleted supernatant (−). This analysis was performed after 12 h of HGF treatment. Data are the means ± SD (error bars) of three independent experiments, performed in duplicate. ***$p < 0.001$ and *$p < 0.05$. (L) Tubulogenesis assay in MDA-MB-435 cells expressing a scrambled shRNA (−) or the ROBO-1–specific shRNA B (+) in the presence of Slit-2–containing (+) or Slit-2–depleted supernatant (−), with or without HGF. The micrographs show representative 10-d-old colonies. Bar, 20 µm. Morphometric analysis is in the bottom panel. n.d., not determined.

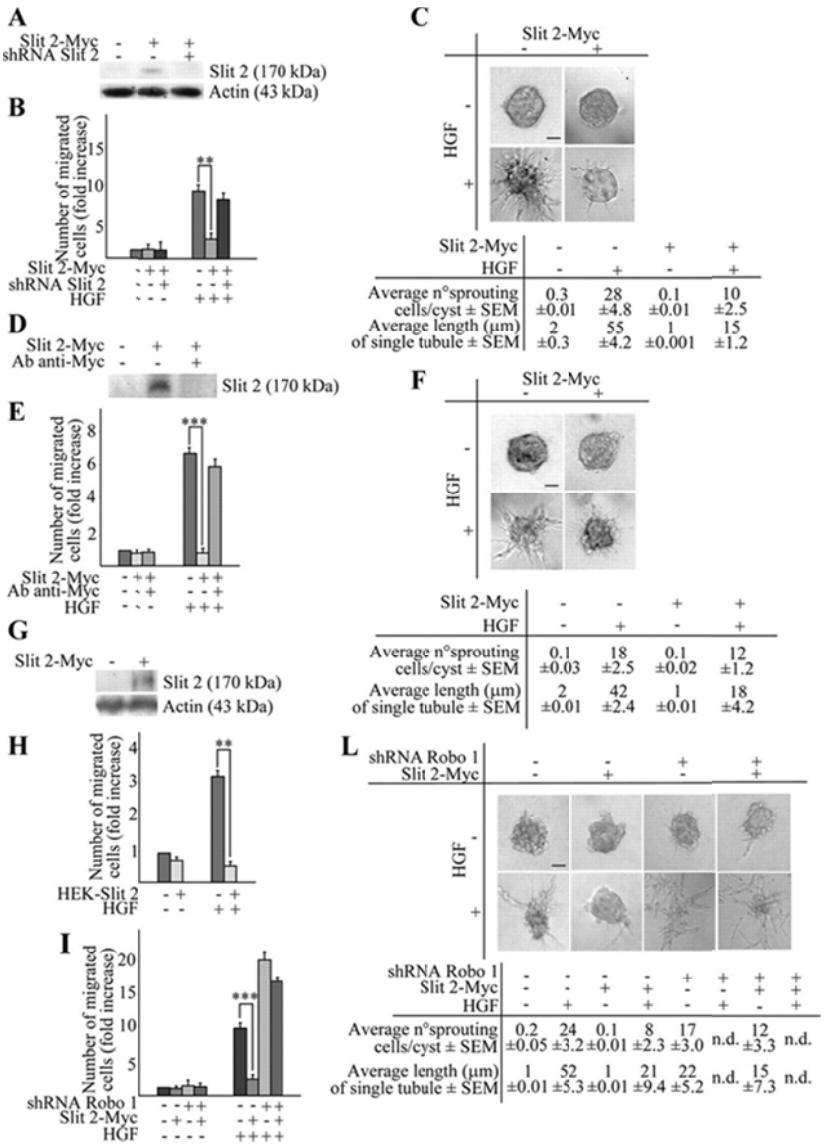

For exogenous administration of the Slit-2 ligand, we first transduced CHO cells with the retroviral Slit-2-Myc construct and then recovered and concentrated the supernatant of these cells. In control experiments, we used medium conditioned by CHO cells secreting Slit-2-Myc after depletion of the soluble Slit protein by anti-Myc immunoprecipitation (Figure 3D). The analysis of anisotropic cell migration showed that, in the presence of soluble Slit-2, wild-type MDA-MB-435 cells did not migrate toward the HGF source. On the contrary, HGF stimulation in the presence of mock medium or the Slit-2–depleted medium resulted in a significant rate of migration, similar to that observable after administration of HGF alone (Figure 3E). In line with that detected with Slit-2–overexpressing MDA-MB-435 cells, HGF was unable to induce a consistent tubulogenic activity in the presence of Slit-2–conditioned medium, whereas it did stimulate robust collagen invasion in the presence of the Slit-2–depleted medium (Figure 3F). Next, we evaluated the ability of exogenous Slit-2 to hamper HGF-dependent cell migration in coculture experiments by using HEK cells expressing Slit-2. In this condition, HEK cells were transduced with the recombinant Slit-2-Myc retroviral construct (Figure 3G). Control or Slit-2–expressing HEK cells were then seeded in the lower compartment of a transwell chamber, whereas wild-type MDA-MB-435 cells were positioned in the upper compartment. Also in this setting, the migration of wild-type MDA-MB-435 cells in response to HGF was strongly inhibited in the presence of Slit-2–secreting HEK cells but not in the presence of control HEK cells (Figure 3H). Finally, we assessed whether the inhibitory effects caused by Slit-2 overactivation were in fact mediated by Robo receptors. Accordingly, we treated cells transduced with a scrambled shRNA or with Robo-1–specific shRNAs with supernatants derived from Slit-2–expressing CHO cells. In control experiments, we used the same medium after Slit-2 depletion by anti-Myc immunoprecipitation. In anisotropic conditions, lack of Robo-1 function potently rescued the impairment of HGF-dependent cell migration produced by exogenous Slit-2 (Figure 3I). Similar results were obtained in three-dimensional collagen assays (Figure 3L). In summary, these findings indicate that either the autocrine or paracrine potentiation of Slit signaling dramatically impairs HGF-induced cell migration, invasion, and branching morphogenesis. This inhibitory activity is predominantly transduced by the Robo-1 receptor.

Effects of the Modulation of the Slit/Robo Pathway on HGF-dependent Responses in Carcinoma Cells

We decided to extend our observations to other neoplastic cell lines that, different from MDA-MB-435, are of epithelial origin, express the junctional adhesion molecule E-cadherin and grow as compact aggregates with well-defined intercellular contacts (Nishimura et al., 2003; DiFeo et al., 2006). Specifically, we examined Skov-3 (ovarian carcinoma) and Hec-1A (endometrial carcinoma). Given the major role of Slit-2 in dictating selective and dominant developmental fates in mammalian tissues where other Slit and Robo members are coexpressed (Wong et al., 2002), we reasoned that decreasing or augmenting the specific activity of Slit-2 would be sufficient to obtain a consistent biological readout in these two cell lines, despite the presence of other Slit and Robo variants (Figure 1A). Similar to that reported for MDA-MB-435, Slit-2 down-regulation enhanced the anisotropic migration of both Skov-3 and Hec-1A toward HGF, whereas Slit-2 overexpression reduced it (Figure 4, A and B, and Supplemental Figure 1). Analogous results were obtained when monitoring random migration under isotropic conditions of HGF concentration (Figure 4, C and D) and when analyzing the HGF-dependent cells' tubulogenic activity in three-dimensional collagen invasion assays (Figure 5, A and B). In this latter case, Slit-2 down-regulation also induced the basal sprouting of tubules in the absence of HGF, a phenotype that was particularly evident in Hec-1A cells and paralleled that observed in Slit-2–deficient MDA-MB-435 cells (Figure 1E).

Table 1. Expression of Slit-2 and Robo-1 in human cancer cells

Expression of Slit-2 and Robo-1 in human cancer cells

Cell line	Tumor derivation	Slit-2	Robo-1
U-87	Glioblastoma	−	+
RT-112	Bladder carcinoma	−	±
RKO	Colon carcinoma	−	+
DLD-1	Colon carcinoma	−	−
HCT-116	Colon carcinoma	+	−

Cell line	Tumor derivation	Slit-2	Robo-1
HT-29	Colon carcinoma	–	–
LoVo	Colon carcinoma	–	–
N87	Gastric carcinoma	–	–
A431	Squamous cell carcinoma	–	+
Skov-3	Ovarian carcinoma	+	+
HeLa	Uterine cervix carcinoma	+	+
MDA-MB-435	Melanoma	+	+
Hec-1A	Endometrial carcinoma	+	+
769-P	Renal carcinoma	+	+

Figure 4. Manipulation of Slit-2 levels in Skov-3 and Hec-1A cells affects HGF-dependent cell motility. (A and B) Anisotropic migration of Skov-3 (A) and Hec-1A (B) cells expressing an empty control vector, the SLIT-2 shRNA or Slit-2-Myc after 12 h of HGF treatment. Data are the means ± SD (error bars) of three independent experiments performed in duplicate. *p < 0.05 and **p < 0.01. (C and D) Distance covered in 36 h by Skov-3 (C) and Hec-1A (D) expressing an empty control vector, the SLIT-2 shRNA or Slit-2-Myc in the absence or presence of isotropic concentrations of HGF. The average values ± SEM, expressed in micrometers, derive from analysis of 10 cells for each experimental condition. This experiment was repeated three times in duplicate. (E and F) Rates of wound repair in scratch assays of Skov-3 (E) and Hec-1A (F) cells in the presence (continuous lines) or absence (dotted lines) of HGF. Green, mock cells. Blue, cells expressing the anti-Slit-2 shRNA. Red, cells overexpressing Slit-2-Myc. Also see Supplemental Figure 2.

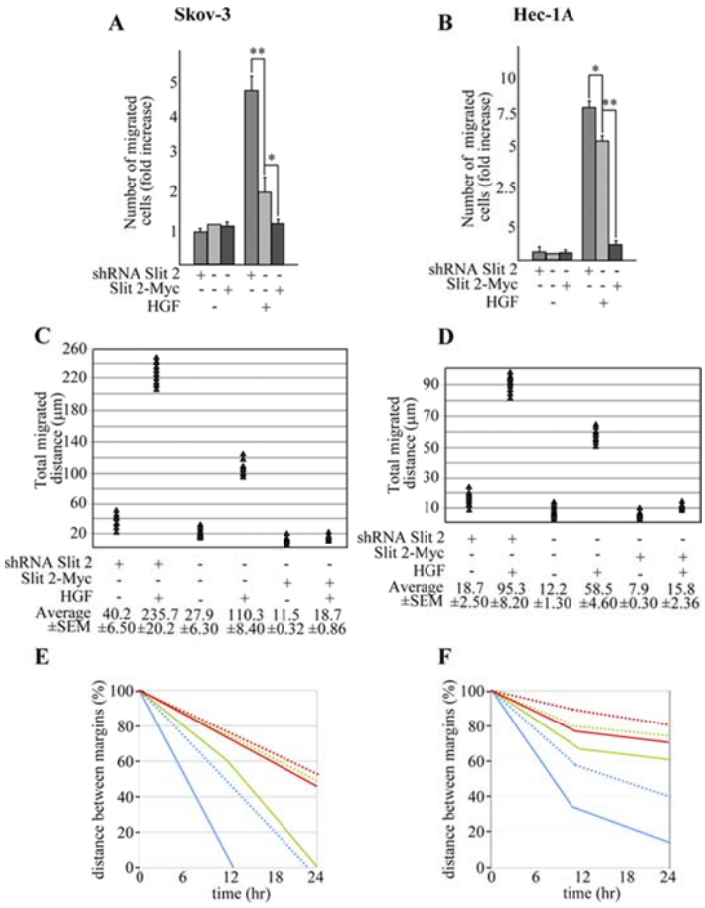

Figure 5. Manipulation of Slit-2 levels in Skov-3 and Hec-1A cells affects HGF-dependent collagen invasion. (A and B) Tubulogenesis assay in Skov-3 (A) and Hec-1A (B) cells expressing an empty control vector, the SLIT-2 shRNA or Slit-2-

Myc. Cells were treated with vehicle (−) or with HGF (+). The micrographs show representative 4-d-old colonies for Skov-3 and 2-d-old colonies for Hec-1A. Bar, 10 μm. Morphometric analysis is in the bottom panel. n.d., not determined.

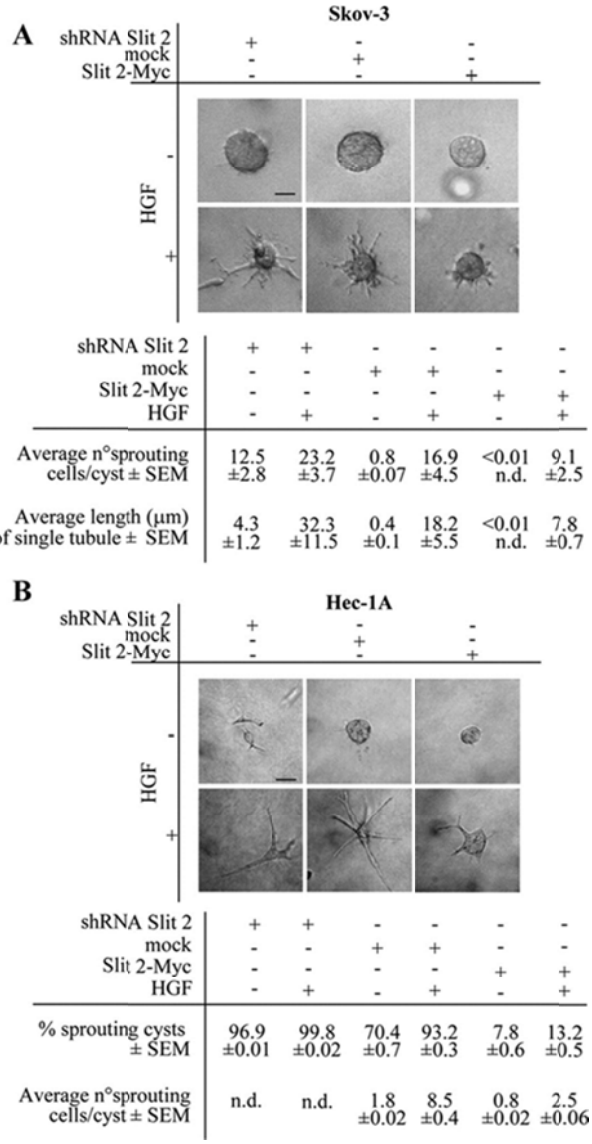

shRNA Slit 2	+	+	-	-	-	-
mock	-	-	+	+	-	-
Slit 2-Myc	-	-	-	-	+	+
HGF	-	+	-	+	-	+
Average n°sprouting cells/cyst ± SEM	12.5 ±2.8	23.2 ±3.7	0.8 ±0.07	16.9 ±4.5	<0.01 n.d.	9.1 ±2.5
Average length (μm) of single tubule ± SEM	4.3 ±1.2	32.3 ±11.5	0.4 ±0.1	18.2 ±5.5	<0.01 n.d.	7.8 ±0.7

shRNA Slit 2	+	+	-	-	-	-
mock	-	-	+	+	-	-
Slit 2-Myc	-	-	-	-	+	+
HGF	-	+	-	+	-	+
% sprouting cysts ± SEM	96.9 ±0.01	99.8 ±0.02	70.4 ±0.7	93.2 ±0.3	7.8 ±0.6	13.2 ±0.5
Average n°sprouting cells/cyst ± SEM	n.d.	n.d.	1.8 ±0.02	8.5 ±0.4	0.8 ±0.02	2.5 ±0.06

The fact that Skov-3 and Hec-1A form tightly packed epithelial sheets allowed us to scrutinize the effects of dosing Slit-2 levels in scratch assays. Again, abatement of Slit-2 expression accelerated both the intrinsic and the HGF-induced motility of Skov-3 so that the scratch was completely repaired after 12 h of HGF treatment. Conversely, increased expression of Slit-2 almost immobilized the cells, and wound repair was not completed even after 24 h of HGF stimulation (Figure 4E and Supplemental Figure 2). The spontaneous migration rate of Hec-1A seemed to be less intense than that of Skov-3. However, also in this case, Slit-2–deficient cells tended to repair the wound more efficiently than mock cells, both under basal conditions and especially in the presence of HGF. In contrast, Slit-2–overexpressing cells moved at a slower pace (Figure 4F and Supplemental Figure 2). Together, these results indicate that Slit-2 can profoundly influence HGF-dependent cell migration and morphogenesis in different neoplastic contexts and in different cellular typologies.

Effects of the Modulation of the Slit/Robo Pathway on HGF-dependent Responses in Polarized Epithelial Cells

HGF can induce motility, invasion and tubulogenesis in several cell types. However, the best-studied cellular model in which to assess the motogenic and morphogenetic properties of this cytokine is represented by the canine kidney cell line MDCK (Stoker et al., 1987; Montesano et al., 1991). On such premises, we decided to include MDCK cells in our analysis. In these cells, the transcriptional profile of the various members of the Slit/Robo family, as assessed by RT-

PCR, included all the three Slit isoforms (Slit-1, Slit-2, and Slit-3) and three of four Robo homologues (Robo-1, Robo-3, and Robo-4) (Figure 6A).

Figure 6. Down-regulation of Slit-2 or Robo-1 in MDCK cells potentiates HGF-dependent cell migration and weakens cell-cell contacts. (A) Endpoint RT-PCR expression of SLIT and ROBO genes in MDCK cells; (−) PCR reaction performed without template. (B) Variations of SLIT-2 mRNA in MDCK cells in the following experimental conditions: wild-type cells (−); cells transduced with a retroviral construct expressing the shRNA-A against human SLIT-2, targeting a sequence that does not match the corresponding canine sequence (therefore, shRNA-A was used as a control in MDCK cells); cells transduced with the ShRNA-B against human SLIT-2, targeting a sequence that is conserved in the corresponding canine cDNA. Data are the means ± SD (error bars) of five independent experiments, performed in triplicate. (C) Variations of ROBO-1 mRNA in MDCK cells in the following experimental conditions: wild-type cells (−); cells transduced with a lentiviral construct expressing a scrambled shRNA sequence (ctr); cells transduced with the shRNA-C against human ROBO-1, targeting a sequence that is conserved in the corresponding canine cDNA. Data are the means ± SD (error bars) of four independent experiments, performed in triplicate. (D) Anisotropic migration of MDCK cells expressing the control (−) or the SLIT-2–specific (+) shRNA after 12 h of HGF. Data are the means ± SD (error bars) of three independent experiments performed in duplicate. *$p < 0.05$. (E) Anisotropic migration of MDCK cells expressing the control (−) or the ROBO-1–specific shRNA C (+) after 12 h of HGF. Data are the means ± SD (error bars) of three independent experiments performed in triplicate. **$p < 0.01$. (F) Scatter assay in MDCK cells expressing the control (−) or the Slit-2–specific shRNA (+), treated with HGF and observed at different time points. Also see Supplemental Movie 1. Bar, 13 μm. (G) Hanging-drop adhesion assay in control (−) or Slit-2–deficient (+) MDCK cells. Bar, 20 μm. (H) Expression of E-cadherin and actin (as a loading control) in control (−) and Slit-2–deficient (+) MDCK cells. (I) Time course analysis of E-cadherin distribution in control (−) and Slit-2–deficient (+) MDCK cells after HGF stimulation (40 ng/ml) for the indicated times. The intercellular pattern of E-cadherin in cells with reduced Slit-2 levels is basally weaker and discontinuous (arrowhead), with only a few cells displaying linear accumulation of E-cadherin (asterisk). Bar, 9 μm.

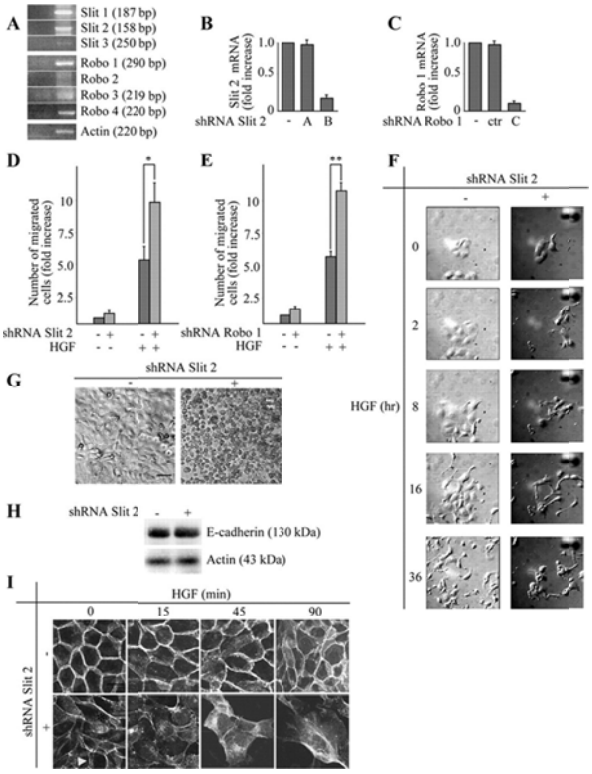

In accordance with the data obtained in MDA-MB-435, Slit-2–deficient MDCK cells (Figure 6B) exhibited an enhanced motogenic response to an anisotropic gradient of HGF compared with cells expressing a control, nontargeting shRNA (Figure 6D). Similar results were obtained upon shRNA-mediated down-regulation of Robo-1 (Figure 6, C and E). We

then monitored the migration of MDCK cells expressing the control or the Slit-2–specific shRNA by time-lapse videomicroscopy. Under isotropic conditions of HGF concentration, Slit-2–deficient cells started dismantling cell-cell contacts earlier than control cells, emitted longer cytoplasmic protrusions and accelerated their initial detachment from the primary colony (Figure 6F and Supplemental Movie 1). These results suggest that Slit-2 silencing goes along with a structural fragility of intercellular junctions, which predisposes the cells to a more rapid acquisition of migratory properties in response to HGF motogenic signals. To test this hypothesis, we carried out aggregation assays in hanging drop cultures (Thoreson et al., 2000), designed to compare the strength of the intercellular adhesions in control or Slit-2–deficient MDCK cells (Figure 6G). As expected, control cells formed tightly compacted aggregates, whereas Slit-2–deficient cells associated only loosely. Western blot analysis of E-cadherin expression in cell lysates obtained from the hanging drop cultures showed no substantial differences in the expression levels of this protein in control versus Slit-2–deficient cells (Figure 6H). However, immunofluorescence staining for E-cadherin localization in MDCK cell colonies before administration of HGF revealed a discontinuous junctional pattern in cells with reduced levels of Slit-2, which suggests an impaired organization of intercellular adhesion complexes. Accordingly, HGF induced a prompt disappearance of E-cadherin from cell–cell contacts in Slit-2–deficient cells. Such delocalization occurred with slower kinetics in control cells (Figure 6I). All in all, the general impression was that reduction of Slit-2 levels induces a "premotile" phenotype that primes cells for rapid and efficient cell–cell dissociation and scattering in response to HGF; thus, Slit-2–deficient cells show basal morphological characteristics similar to those of mock cells involved in the early phases of HGF-triggered motility. To extend this observation, we used confocal microscopy to analyze the subcellular distribution of other molecular markers of lateral contacts (namely, β-catenin and the tight junction protein ZO-1) and that of vinculin, a major component of cell-substrate adhesion. Again, we noticed that the junctional immunoreactivity for β-catenin and ZO-1 was already weaker in quiescent Slit-2–deficient cells compared with mock cells, and the lateral enrichment of both molecules was further reduced after a brief (60-min) exposure to HGF (Figure 7, A and B). Accordingly, mock cells displayed a ventral dot-like pattern of vinculin localization, which indicates association with focal contacts. As expected, HGF-induced cell spreading was accompanied by a cytoplasmic dispersal of vinculin, together with a minor redistribution at residual cell–cell contacts and at leading edges. This topography was already present in nonstimulated Slit-2–deficient cells, and vinculin cytoplasmic diffusion was exacerbated by HGF (Figure 7C).

Figure 7. Distribution of adhesion markers in MDCK cells with normal or reduced levels of Slit-2. Double staining for actin and molecular markers of cell–cell contacts (A and B) or cell-substrate adhesion (C) in mock and shRNA-SLIT-2 cells in the presence (+) or absence (−) of HGF (40 ng/ml for 60 min). The lateral enrichment of β-catenin (A) and ZO-1 (B) is basally reduced in Slit-2–deficient cells (arrowhead for β-catenin and arrows for ZO-1) and further decreases after short-term HGF stimulation. Similarly, vinculin immunoreactivity (C) at focal contacts is impaired in Slit-2–deficient cells, with further cytoplasmic redistribution after HGF. β-Catenin and ZO-1 staining is from apical optical sections; vinculin staining is from basal sections. Bar, 4 μm (color) and 6 μm (black and white).

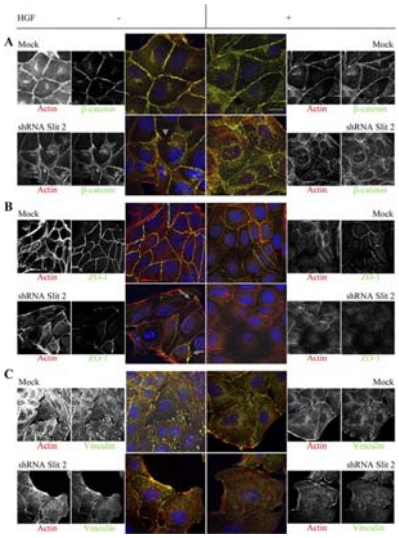

In an opposite perspective, we increased Slit-2 signaling by supplying this molecule in the extracellular environment, using either the conditioned medium derived from Slit-2-Myc-expressing CHO cells or cocultures with Slit-2-Myc HEK cells. Wild-type MDCK cells treated with soluble, CHO-derived Slit-2 protein displayed a 12-fold reduction in HGF-dependent migration (across transwell filters) compared with cells exposed to mock or Slit-2–depleted supernatants (Figure 8A). When the migration assay was performed in the presence of Slit-2-Myc–expressing HEK cells, MDCK cells were threefold less efficient in the migratory response to HGF than MDCK cells cocultured with control HEK cells (Figure 8B). Similarly, HGF-induced invasion of wild-type MDCK cells embedded in collagen gels was severely impaired upon concomitant administration of soluble Slit-2 (Figure 8C). Then, we monitored if the inhibition of cell migration and branching morphogenesis due to Slit-2 overexpression was in fact mediated by Robo receptors. Accordingly, we treated cells transduced with a scrambled shRNA or with Robo-1–specific shRNAs (Figure 6C) with supernatants derived from Slit-2–expressing CHO cells or with control, Slit-2–depleted supernatants. Similar to MDA-MB-435 cells, lack of Robo-1 function rescued the impairment of HGF-dependent cell migration and collagen invasion produced by exogenous Slit-2 (Figure 8, D and E). Finally, in scratch assays, Slit-2 down-regulation accelerated, whereas Slit-2 overexpression retarded, the time required to close the wounds, both under basal conditions and upon HGF stimulation (Figure 8F and Supplemental Figure 2).

Figure 8. Exogenous Slit-2 inhibits HGF-dependent cell migration, tubulogenesis, and wound repair in MDCK cells. (A) Anisotropic migration of MDCK cells in the presence of CHO-derived control supernatant, Slit-2-containing supernatant, or Slit-2–depleted supernatant. This analysis was performed after 12 h of HGF treatment. Data are the means ± SD (error bars) of three independent experiments performed in duplicate. ***$p < 0.001$. (B) Anisotropic migration of MDCK cells cocultured with HEK cells expressing or not expressing Slit-2-Myc. Cell migration was quantitated after 12 h of HGF treatment. Data are the means ± SD (error bars) of two independent experiments performed in duplicate. **$p < 0.01$. (C) Tubulogenesis assay in MDCK cells in the presence of Slit-2–depleted (−) or Slit-2–containing (+) medium, with or without HGF. The micrographs show representative 7-d-old colonies. Bar, 30 μm. Morphometric analysis is in the right panel. (D) Anisotropic migration of MDCK cells expressing a scrambled shRNA (−) or the ROBO-1–specific shRNA C (+) in the presence of Slit-2–containing (+) or Slit-2–depleted supernatant (−). This analysis was performed after 12 h of HGF treatment. Data are the means ± SD (error bars) of three independent experiments performed in duplicate. ***$p < 0.001$. (E) Tubulogenesis assay in MDCK cells expressing a scrambled shRNA (−) or the ROBO-1–specific shRNA C (+) in the presence of Slit-2–containing (+) or Slit-2–depleted supernatant (−), with or without HGF. The micrographs show representative 4-d-old colonies. Bar, 20 μm. Morphometric analyses are shown. n.d., not determined. (F) Rates of wound repair in scratch assays with (continuous lines) or without (dotted lines) HGF. Green, mock cells. Blue, cells expressing the anti-Slit-2 shRNA. Red, cells overexpressing Slit-2. Also see Supplemental Figure 2.

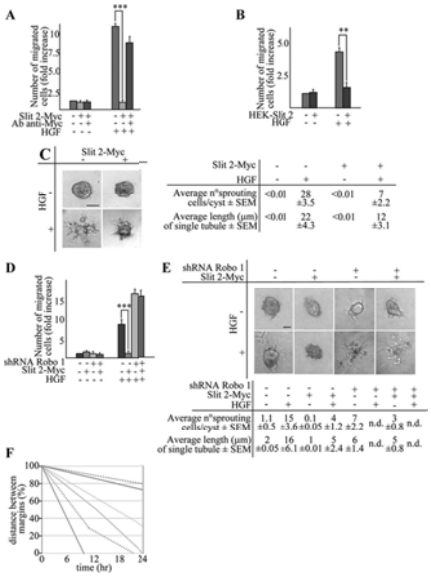

In sum, modulation of Slit-2/Robo-1 function in MDCK cells recapitulates the findings obtained with the other cell lines, extending the concept that Slit/Robo signaling limits motility, matrix invasion and morphogenesis of epithelial cells.

Slit-2 Affects HGF-dependent Activation of Cdc-42 and Rac-1

Several mechanisms can be evoked to explain the inhibitory role that the Slit/Robo system exerts on HGF-induced cell motility and branching morphogenesis. For example, a direct interaction between Slit and Met could down-modulate Met responses after HGF treatment. However, by pool-down experiments using soluble tagged Slit-2 protein or by coimmunoprecipitation experiments using cells overexpressing Slit-2-Myc, we were unable to demonstrate a physical association between Slit and Met or HGF/Met. Moreover, Slit-2 did not prevent Met activation as it did not affect Met phosphorylation after HGF treatment (Supplemental Figure 3). Another putative mechanism might rely on the capacity of Slit-2 to inhibit cell proliferation and/or to increase apoptosis. This possibility can be excluded as well; in fact, Slit-2 displays a modest proapoptotic activity together with a minor antiproliferative effect (Supplemental Figure 4); however, these activities are not sufficient per se to justify the almost complete abrogation of HGF-dependent cell motility and branching morphogenesis observed in cells overexpressing Slit-2. Finally, one could speculate that the Slit/Robo and the HGF/Met pathways interact on common downstream target molecules directly involved in cytoskeletal dynamics. An intriguing observation made on Slit-2–deficient MDCK cell was that, in addition to the vulnerable structure of intercellular contacts and the prompt acquisition of HGF-induced motile properties, these cells formed filopodial extensions at their leading edges shortly after HGF stimulation (Figure 9A). In contrast, control MDCK cells responded to HGF with the production of large lamellipodia exhibiting actin enrichment at the front, consistent with previous observations (Koch et al., 2005). An analogous phenotype could be also detected in MDA-MB-435 cells. In this cell line, unstimulated control cells seemed to be firmly spread to the substrate, with robust actin cables running through the cytoplasm. After a brief exposure to HGF, the cells became elongated and redistributed their actin cytoskeleton in linear or dotted structures close to the newly-formed front of migration. This phenotype was already present, under basal conditions, in Slit-2–deficient cells. In these cells, similar to that observed in MDCK, HGF treatment led to the generation of an array of filopodial spikes (Figure 9A).

Figure 9. Slit-2 affects HGF-dependent actin reorganization and activation of Cdc-42 and Rac-1. (A) Organization of the actin cytoskeleton in MDCK (left) and MDA-MB-435 (right) expressing normal or reduced levels of Slit-2, in the presence or absence of HGF (for 90 min). The actin cytoskeleton was visualized by TRITC-conjugated phalloidin. Bar, 4 μm at low magnification and 1.5 μm at high magnification. (B–E) Time course analysis of Cdc-42 (B and D) and Rac-1 (C and E) activation in MDA-MB-435 cells in which Slit-2 expression was either down-regulated (B and C) or enhanced (D and E). In each panel, the top blot corresponds to the pull-down experiment using PAK-conjugate beads; the bottom blot represents total cell lysates as loading controls. The intensities of each band in the pool-down experiments were normalized with respect to the corresponding band in the whole cell extracts. Numbers under the representative blots are the means ± SD of three independent experiments.

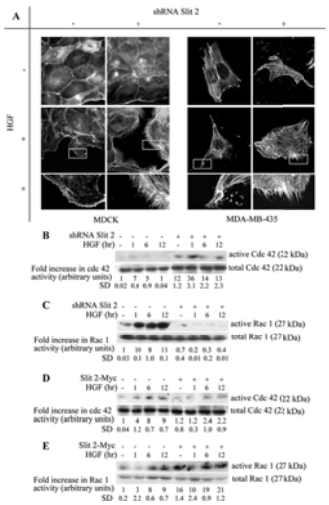

During axon guidance the repulsive action of Slit-2 is mediated, among other factors, by changes in the activity of Cdc-42 and Rac-1, two members of the Rho-like family of small GTPases (Wong et al., 2001; Fan et al., 2003; Yang and Bashaw, 2006). Because Rac-1 is required for production and stabilization of cell–cell contacts (Sahai and Marshall, 2002) and Cdc-42 is a well-known inducer of filopodia formation (Nobes and Hall, 1995), we speculated that the reduced strength of intercellular junctions and the increased production of filopodia observed in Slit-2–deficient cells could be due to a Slit-2–dependent modulation of Rac-1 and Cdc-42 activities, which interferes with HGF-triggered motility. To test this hypothesis, we monitored HGF-dependent activation of Cdc-42 and Rac-1 in control and Slit-2–deficient MDA-MB-435 cells. We chose this cell line because these cells express higher amounts of both Cdc-42 and Rac-1 compared with Skov-3, Hec-1A, and MDCK cells,. In their active, GTP-bound form, both Rac-1 and Cdc-42 bind directly to p21-activated kinase-1 (PAK-1) (Burbelo et al., 1995). We thus analyzed Cdc-42 and Rac-1 activation by pool-down experiments using the Cdc42/Rac interactive binding domain of PAK-1. In the absence of HGF, the basal activity of Cdc-42 was higher in Slit-2–deficient cells (Figure 9B), whereas the activity of Rac-1 was higher in control cells (Figure 9C). The HGF-dependent activation of Cdc-42 was only modestly augmented in control cells, whereas it was potently increased in Slit-2–deficient cells (Figure 9B). Conversely, HGF treatment further increased Rac-1 activation in control cells, but it was unable to induce any substantial stimulation of Rac-1 in cells with reduced levels of Slit-2 (Figure 9C). Opposite (and complementary) results were obtained when examining MDA-MB-435 cells overexpressing Slit-2-Myc. In this setting, autocrine overproduction of Slit-2 almost totally suppressed Cdc-42 activation (Figure 9D), whereas it hyperinduced the basal and (to a much lower extent) HGF-triggered activity of Rac-1 (Figure 9E). In an attempt to provide a causal link between the Slit-2-dependent regulation of Rho-like GTPases and HGF-dependent cell motility, we decided to perturb the activity of Cdc-42 in MDA-MB-435 cells with normal or reduced levels of Slit-2. We reasoned that, if the increased motogenic and invasive response observed in cells with reduced levels of Slit-2 is due to the up-regulation of Cdc-42, then inhibition of Cdc-42 should reduce HGF-dependent cell motility in Slit-2–deficient cells. Conversely, constitutive activation of Cdc-42 in cells overexpressing Slit-2 should restore cell migration. Accordingly, we transiently transfected Slit-2–deficient and Slit-2–overexpressing MDA-MB-435 cells with an HA-tagged dominant-negative variant of Cdc-42 (Cdc-42-DN-HA) or with a FLAG-tagged, constitutively active form of Cdc-42 (Cdc-42-gof-Flag), respectively (Supplemental Figure 5). In a transwell assay, alteration of Cdc-42 activity affected HGF-dependent migration in both Slit-2–deficient and Slit-2–overexpressing cells, in accordance with the well-established role of Cdc-42 as a master regulator of cytoskeletal dynamics and cell motility. However, although Cdc-42 inhibition strongly impaired migration in Slit-2–deficient cells, the constitutively active Cdc-42 mutant was only partially effective in increasing the migratory ability of cells overexpressing Slit-2 (Figure 10, A and B). This suggests that the activity of Cdc-42 in stimulating cellular locomotion is critical whenever Slit-2 is silenced but is not sufficient to overcome the migratory impairment induced by Slit-2 overexpression.

Figure 10. Deregulated activation of Cdc-42 and Rac-1 strongly impairs HGF-dependent migration in MDA-MB-435 cells and junction integrity in MDCK cells harboring altered expression of Slit-2. Anisotropic migration in response to a 12-h treatment of HGF in MDA-MB-435-Slit-2–deficient cells in the presence or absence of Cdc-42-DN-HA (A) and Rac-1-gof-Myc (G) or MDA-MB-435-Slit 2-Myc cells expressing either Cdc-42-gof-FLAG (B) or Rac-1-DN-Myc (H). Data are the means ± SD (error bars) of three independent experiments, performed in duplicate. Hanging-drop adhesion assay in Slit-2-deficient (E and C) or Slit-2–overexpressing (F and D) MDCK cells transfected with Rac-1-gof-Myc (C), Rac-1-DN-Myc (D), Cdc-42-DN-HA (E), and Cdc-42-gof-Flag (F). Bar, 20 μm.

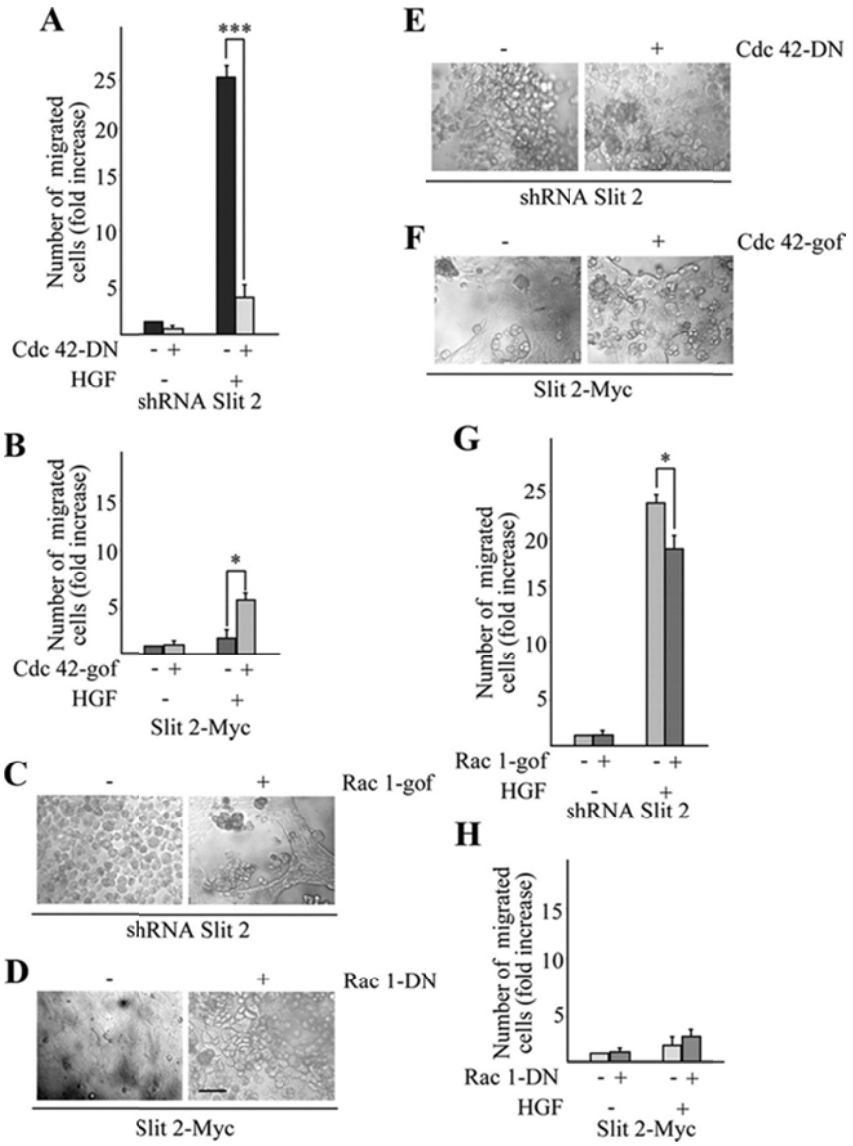

Complementary to this, if Slit-2 reinforces cell–cell contacts through activation of Rac-1, then Rac-1 inhibition should weaken contact integrity of Slit-2–overexpressing cells, whereas constitutive activation of Rac-1 should rescue the intercellular junction fragility typical of Slit-2–deficient cells. Thus, we transiently expressed dominant negative or constitutively active forms of Rac-1 (Rac-1-DN-Myc and Rac-1-gof-Myc) in Slit-2–overexpressing or Slit-2–deficient MDCK cells, respectively (Supplemental Figure 5). As expected, using aggregation assays in hanging drop cultures, expression of Rac-1-DN-Myc resulted in the disruption of intercellular contacts in cell overexpressing Slit-2, whereas Rac-1-gof-Myc rescued the dissociated phenotype of cells lacking Slit-2 (Figure 10, C and D). Notably, in either cell transfectants, alteration of Cdc-42 activity did not influence cell–cell contact integrity (Figure 10, E and F) and perturbation of Rac-1 affected only modestly cell migration (Figure 10, G and H). These results indicate that the Slit/Robo system modulates the activity of Rho-like GTPases in epithelial cells by constraining the activity of Cdc-42 in cell migration and potentiating the activity of Rac-1 in cell–cell contact dynamics. However, in Slit-2-overexpressing cells, active Cdc-42 is not sufficient to fully rescue cell migration and abrogation of Rac-1 activity does not lead to an overt motile phenotype. This suggests that the role of Cdc-42 as a driving force for cell movement becomes evident only upon Rac-1 down-modulation, when intercellular junctions get disorganized. This might explain the effects on the integrity of cell–cell junctions and the organization of the actin cytoskeleton observed when we disrupt Slit/Robo signaling.

DISCUSSION

During organ development and tissue remodeling, positional information is often tuned by the concerted activity of paracrine stimulatory cues, released distally, and autocrine inhibitory morphogens, which act locally to restrain migration toward the external attractant source. In this article, we show that immortalized, nontransformed epithelial cells and cancerous cell lines empower the Slit-2/Robo-1 signaling system to mitigate HGF-dependent migration, matrix invasion, and branching morphogenesis. Our results are in concordance with previous studies demonstrating that the Slit/Robo system is required for the spatial constraint and the proper obliteration of supernumerary structures during development, including the bronchial tree and the ureteric buds (Xian et al., 2001; Grieshammer et al., 2004).

The positional restriction exerted by the Slit/Robo system loop might have important implications as a safeguard mechanism during cancer invasion and metastasis. Indeed, our results suggest that the xenophilic propensity of malignant cells could be negatively regulated, or at least spatially modulated, by the endogenous activity of the Slit/Robo system. This line of thinking fits with the observations that Slit-2 inhibits CXCL12-induced chemotaxis in breast carcinoma cells (Prasad et al., 2004) and that endogenous levels of CXCL12 antagonize the repellent effects of Slit/Robo signaling during retinal axon pathfinding in zebrafish (Chalasani et al., 2007). Moreover, the Slit genes frequently undergo epigenetic inactivation in a vast number of human cancers (Dallol et al., 2002, 2003a,b; Astuti et al., 2004; Dickinson et al., 2004). It is tempting to speculate that, during the evolutionary trajectory of an incipient cancer cell, Slit silencing provides a selective advantage for neoplastic progression through disengagement of anti-invasive cues. This activity is likely to be corroborated by concomitant stimulation of cell accretion, because Slit 2 has been demonstrated to exert antimitotic and proapoptotic effects (Dallol et al., 2002, 2003b); indeed, we also found that Slit 2 down-regulation partially enhances, whereas Slit 2 overexpression decreases, the viability of the cell lines tested in this study, although to different extents (Supplemental Figure 3).

The notion that the Slit genes might hinder full implementation of the malignant phenotype is in contrast with the finding that tumors expressing Slit-2 can attract endothelial cells expressing Robo-1, thus inducing angiogenesis and favoring cancer growth (Wang et al., 2003). In the absence of animal models in which to investigate the heterotypic communications between tumor, endothelial, and stromal cells on conditional backgrounds of Slit and Robo expression, it is difficult to assess the relative contribution of Slit as a repellent for the tumor and an attractant for endothelial cells. However, one could argue that the net effect of Slit activity within the tumor likely results from the reciprocal stoichiometry of autocrine versus paracrine stimulation, the expression levels of the Robo receptors in the different cell types, and the synergistic or antagonistic interactions with other morphogens such as ephrins, semaphorins, and angiogenic factors (Bissell and Radisky, 2001).

The anti-migratory activity of Slit-2 derives, at least partially, from the inhibition of actin-based protrusive forces. Indeed, when Slit-2 is down-regulated, HGF stimulation results in the production of a copious amount of filopodia at the leading edge of cells as a prelude for efficient locomotion (Figure 9A). In response to HGF, this enhanced filopodia formation in the absence of Slit/Robo signaling is accompanied by an increased activity of Cdc-42, whereas Slit-2 overexpression greatly reduces HGF-dependent activation of Cdc-42 (Figure 9, B and D). Consistent with these data, it has been demonstrated that the repelling activity of Slit during neuronal migration requires the interaction between the intracellular domain of Robo-1 and a novel family of Rho GTPase-activating proteins (srGAPs) and that this interaction specifically inhibits Cdc-42 (Wong et al., 2001). Similarly, it has been reported that Slit-2–dependent inhibition of medulloblastoma cell invasion goes along with Cdc-42 down-regulation (Werbowetski-Ogilvie et al., 2006).

Besides impairing actin-rich motility structures, Slit-2 also potentiates the adhesive strength of cadherin-mediated intercellular contacts, making multicellular colonies less prone to cell–cell dissociation and scattering. This activity is possibly mediated by Slit-induced upregulation of Rac-1, as we observed by genetic manipulation of Slit-2 expression levels (Figure 9, C and E, and Fig. 10, C and D). Accordingly, it has been shown that in both mammalian cells and Drosophila embryos Slit activates Rac-1 by recruiting the guanine-nucleotide exchange factor (GEF) Sos to Robo (Fan et al., 2003; Yang and Bashaw, 2006).

Although the general role of Rac-1 in the maturation and stabilization of intercellular contacts is well established, its function in HGF-dependent cell motility is, at first sight, contradictory: on the one hand, overexpression of the Rac-specific GEF Tiam-1 inhibits HGF-induced scattering by increasing E-cadherin–mediated cell–cell adhesion and promoting actin polymerization at cell–cell contacts (Hordijk et al., 1997); on the other hand, HGF induces lamellipodia

formation at the cell's leading edges and cell locomotion by means of Rac-1 activation (Potempa and Ridley, 1998). One hypothesis for this apparent discrepancy, also favored by others (Price and Collard, 2001), is that the pre-existing threshold and the subcellular compartmentalization of Rac-1 activity, as well as the balance between cell–cell and cell–matrix adhesion, could dictate the biological outcome in response to HGF. If Rac-1 is basally very active at cell–cell contacts (a condition that occurs in the presence of elevated levels of Tiam-1 and in the inner part of compact epithelial colonies, where cell–cell interactions prevail over cell–matrix adhesions), then intercellular junctions display a robust mechanical strength that HGF is unable to weaken; conversely, in the presence of a low and diffuse Rac-1 activity (for example, at the periphery of quiescent epithelial colonies, where cell–substrate adhesion dynamics dominate over cell–cell interactions), HGF triggers a Rac-1–dependent focalization of actin polymerization at the free margins of the cells, which start developing lamellipodia protrusions as a prerequisite for cell migration. We postulate that the ability of Slit-2 to augment the basal activity of Rac-1, which cannot be substantially superinduced by HGF stimulation (Figure 9E), shifts the equilibrium toward stabilization of intercellular contacts. This is in line with the observation that overexpression of activated Rac-1 alone (Ridley et al., 1995) is not sufficient to recapitulate HGF-induced cell scattering, possibly because of a more efficient activity on the stabilization of intercellular contacts.

In conclusion, our findings reinforce the idea of fundamental conservation of directional mechanisms for all somatic cells (Wu et al., 2001; Rao et al., 2002) and support the notion that the Slits and the Robos act as general guidance cues, tipping the balance between stimulatory and inhibitory morphogen gradients toward cellular repulsion. This condition, in an autocrine context, leads to the induction of a stationary phenotype which precludes cells from migrating toward motogenic stimuli. It will be interesting to analyze whether such positional constraint will impact tumor metastatization by using in vivo models of cancer progression, and whether the frequently observed epigenetic silencing of Slit-2 will be predictive of bad prognosis and tumor dissemination in human malignancies.

ACKNOWLEDGMENTS

We thank Carla Boccaccio, Andrea Bertotti, and Asha Balakrishnan for critical reading of the manuscript; Damion Milne and Giorgio Giardina for image analysis; the Division of Molecular Angiogenesis for help and collaboration; Raffaella Albano, Laura Palmas and Lara Fontani for technical assistance; and Antonella Cignetto for secretarial assistance. This work was supported by Associazione Italiana per la Ricerca sul Cancro grants (to P.M.C. and L.T.) and a Ministero dell'Istruzione, dell'Università e della Ricerca (PRIN 2004) grant (to L.T.).

Footnotes

Address correspondence to: Maria Cristina Stella (mariacristina.stella@ircc.it) or Livio Trusolino (livio.trusolino@ircc.it)

This article was published online ahead of print in MBC in Press (http://www.molbiolcell.org/cgi/doi/10.1091/mbc.E08-03-0321) on November 12, 2008.

REFERENCES

↵ Astuti D., et al. (2004) SLIT2 promoter methylation analysis in neuroblastoma, Wilms' tumour and renal cell carcinoma. Br. J. Cancer 90:515–521.

↵ Birchmeier C., Gherardi E. (1998) Developmental roles of HGF/SF and its receptor, the c-Met tyrosine kinase. Trends Cell Biol 8:404–410.

↵ Birchmeier C., Birchmeier W., Gherardi E., Vande Woude G. F. (2003) Met, metastasis, motility and more. Nat. Rev. Mol. Cell. Biol 4:915–925.

↵ Bissell M. J., Radisky D. (2001) Putting tumours in context. Nat. Rev. Cancer 1:46–54.

↵ Burbelo P. D., Drechsel D., Hall A. (1995) A conserved binding motif defines numerous candidate target proteins for both Cdc42 and Rac GTPases. J. Biol. Chem 270:29071–29074.

↵ Chalasani S. H., Sabol A., Xu H., Gyda M. A., Rasband K., Granato M., Chien C. B., Raper J. A. (2007) Stromal cell-derived factor-1 antagonizes slit/robo signaling in vivo. J. Neurosci 27:973–980.

↵ Brummelkamp , et al. (2002) A system for stable expression of short interfering RNAs in mammalian cells. Science 296:550–553.

↲ Comoglio P. M., Trusolino L. (2002) Invasive growth: from development to metastasis. J. Clin. Invest 109:857–862.

↲ Dallol A., Da Silva N. F., Viacava P., Minna J. D., Bieche I., Maher E. R., Latif F. (2002) SLIT2, a human homologue of the Drosophila Slit2 gene, has tumor suppressor activity and is frequently inactivated in lung and breast cancers. Cancer Res 62:5874–5880.

↲ Dallol A., Krex D., Hesson L., Eng C., Maher E. R., Latif F. (2003a) Frequent epigenetic inactivation of the SLIT2 gene in gliomas. Oncogene 22:4611–4616.

↲ Dallol A., Morton D., Maher E. R., Latif F. (2003b) SLIT2 axon guidance molecule is frequently inactivated in colorectal cancer and suppresses growth of colorectal carcinoma cells. Cancer Res 63:1054–1058.

↲ Dickinson R. E., Dallol A., Bieche I., Krex D., Morton D., Maher E. R., Latif F. (2004) Epigenetic inactivation of SLIT3 and SLIT1 genes in human cancers. Br. J. Cancer 91:2071–2078.

↲ Dickson B. J., Gilestro G. (2006) Regulation of commissural axon pathfinding by slit and its robo receptors. Annu. Rev. Cell Dev. Biol 22:651–675.

↲ DiFeo A., Narla G., Camacho-Vanegas O., Nishio H., Rose S. L., Buller R. E., Friedman S. L., Walsh M. J., Martignetti J. A. (2006) E-cadherin is a novel transcriptional target of the KLF6 tumor suppressor. Oncogene 25:6026–6031.

↲ Esko J. D., Weinke J. L., Taylor W. H., Ekborg G., Roden L., Anantharamaiah, G, Gawish A. (1987) Inhibition of chondroitin and heparan sulfate biosynthesis in Chinese hamster ovary cell mutants defective in galactosyltransferase I. J. Biol. Chem 262:12189–12195.

↲ Fan X., Labrador J. P., Hing H., Bashaw G. J. (2003) Slit stimulation recruits Dock and Pak to the roundabout receptor and increases Rac activity to regulate axon repulsion at the CNS midline. Neuron 40:113–127.

↲ Grieshammer U., Le Ma, Plump A. S., Wang F., Tessier-Lavigne M., Martin G. R. (2004) SLIT2-mediated ROBO2 signaling restricts kidney induction to a single site. Dev. Cell 6:709–717.

↲ Hordijk P. L., ten Klooster J. P., van der Kammen R. A., Michiels F., Oomen L. C., Collard J. G. (1997) Inhibition of invasion of epithelial cells by Tiam1-Rac signaling. Science 278:1464–1466.

↲ Huber M. A., Kraut N., Beug H. (2005) Molecular requirements for epithelial-mesenchymal transition during tumor progression. Curr. Opin. Cell Biol 17:548–558.

↲ Hussain S. A., et al. (2006) A molecular mechanism for the heparan sulfate dependence of slit-robo signaling. J. Biol. Chem 281:39693–39698.

↲ Koch A., Mancini A., El Bounkari O., Tamura T. (2005) The SH2-domian-containing inositol 5-phosphatase (SHIP)-2 binds to c-Met directly via tyrosine residue 1356 and involves hepatocyte growth factor (HGF)-induced lamellipodium formation, cell scattering and cell spreading. Oncogene 24:3436–3447.

↲ Lecuit T., Lenne P. F. (2007) Cell surface mechanics and the control of cell shape, tissue patterns and morphogenesis. Nat. Rev. Mol. Cell Biol 8:633–644.

↲ Liang Y., Annan R. S., Carr S. A., Popp S., Mevissen M., Margolis R. K., Margolis R. U. (1999) Mammalian homologues of the Drosophila slit protein are ligands of the heparan sulfate proteoglycan glypican-1 in brain. J. Biol. Chem 274:17885–17892.

↲ Maina F., Klein R. (1999) Hepatocyte growth factor, a versatile signal for developing neurons. Nat. Neurosci 2:213–217.

↲ Michieli P., Mazzone M., Basilico C., Cavassa S., Sottile A., Naldini L., Comoglio P. M. (2004) Targeting the tumor and its microenvironment by a dual-function decoy Met receptor. Cancer Cell 6:61–73.

↲ Montesano R., Schaller G., Orci L. (1991) Induction of epithelial tubular morphogenesis in vitro by fibroblast-derived soluble factors. Cell 66:697–711.

↲ Naldini L., Vigna E., Bardelli A., Follenzi F., Galimi F., Comoglio P. M. (1995) Biological activation of pro-HGF (hepatocyte growth factor) by urokinase is controlled by a stoichiometric reaction. J. Biol. Chem 270:603–611.

↲ Nishimura M., Saito T., Yamasaki H., Kudo R. (2003) Suppression of gap junctional intercellular communication via 5' CpG island methylation in promoter region of E-cadherin gene in endometrial cancer cells. Carcinogenesis 24:1615–1623.

↲ Nobes C. D., Hall A. (1995) Rho, rac, and cdc42 GTPases regulate the assembly of multimolecular focal complexes associated with actin stress fibers, lamellipodia, and filopodia. Cell 81:53–62.

↲ Potempa S., Ridley A. J. (1998) Activation of both MAP kinase and phosphatidylinositide 3-kinase by Ras is required for hepatocyte growth factor/scatter factor-induced adherens junction disassembly. Mol. Biol. Cell 9:2185–2200.

↲ Prasad A., Fernandis A. Z., Rao Y., Ganju R. K. (2004) Slit protein-mediated inhibition of CXCR4-induced chemotactic and chemoinvasive signaling pathways in breast cancer cells. J. Biol. Chem 279:9115–9124.

↲ Price L. S., Collard J. C. (2001) Regulation of the cytoskeleton by Rho-like GTPases: implications for tumour cell invasion. Semin. Cancer Biol 11:167–173.

↲ Rao Y., Wong K., Ward M., Jurgensen C., Wu J. Y. (2002) Neuronal migration and molecular conservation with leukocyte chemotaxis. Genes Dev 16:2973–2984.

↲ Ridley A. J., Comoglio P. M., Hall A. (1995) Regulation of scatter factor/hepatocyte growth factor responses by Ras, Rac, and Rho in MDCK cells. Mol. Cell. Biol 15:1110–1122.

↲ Ronca F., Andersen J. S., Paech V., Margolis R. U. (2001) Characterization of Slit protein interactions with glypican-1. J. Biol. Chem 276:29141–29147.

↲ Sahai E., Marshall C. J. (2002) RHO-GTPases and cancer. Nat. Rev. Cancer 2:133–142.

↲ Sander E. E., van Delft S., ten Klooster J. P., Reid T., van der Kammen R. A., Michiels F., Collard J. G. (1998) Matrix-dependent Tiam1/Rac signaling in epithelial cells promotes either cell-cell adhesion or cell migration and is regulated by phosphatidylinositol 3-kinase. J. Cell Biol 143:1385–1398.

↲ Stella M. C., Trusolino L., Pennacchietti S., Comoglio P. M. (2005) Negative feedback regulation of Met-dependent invasive growth by Notch. Mol. Cell. Biol 25:3982–3996.

↲ Stoker M., Gherardi E., Perryman M., Gray J. (1987) Scatter factor is a fibroblast-derived modulator of epithelial cell mobility. Nature 327:239–242.

↲ Thoreson M. A., Anastasiadis P. Z., Daniel J. M., Ireton R. C., Wheelock M. J., Johnson K. R., Hummigbird D. K., Reynolds A. B. (2000) Selective uncoupling of p120(ctn) from E-cadherin disrupts strong adhesion. J. Cell Biol 148:189–202.

↲ Trusolino L., Bertotti A., Comoglio P. M. (2001) A signaling adapter function for α6β4 integrin in the control of HGF-dependent invasive growth. Cell 107:643–654.

↲ Wang B., et al. (2003) Induction of tumor angiogenesis by Slit-Robo signaling and inhibition of cancer growth by blocking Robo activity. Cancer Cell 4:19–29.

↲ Werbowetski-Ogilvie T. E., et al. (2006) Inhibition of medulloblastoma cell invasion by Slit. Oncogene 25:5103–5112.

↲ Wong K., et al. (2001) Signal transduction in neuronal migration: roles of GTPase activating proteins and the small GTPase Cdc42 in the Slit-Robo pathway. Cell 107:209–221.

↲ Wong K., Park H. T., Wu J. Y., Rao Y. (2002) Slit proteins: molecular guidance cues for cells ranging from neurons to leukocytes. Curr. Opin. Genet Dev 12:583–591.

↲ Wu W., Wong K., Chen J. H., Jiang Z. H., Dupuis S. M., Wu J. Y., Rao Y. (1999) Directional guidance of neuronal migration in the olfactory system by the protein Slit. Nature 400:331–336.

↲ Wu J. Y., Feng L. L., Park H. T., Havlioglu N., Wen L., Tang H., Bacon K. B., Jiang Z. H., Zhang X. C., Rao Y. (2001) The neuronal repellent Slit inhibits leukocyte chemotaxis induced by chemotactic factors. Nature 410:948–952.

↲ Xian J., Clark K. J., Fordham R., Pannell R., Rabbitts T. H., Rabbitts P. H. (2001) Inadequate lung development and bronchial hyperplasia in mice with a targeted deletion in the Dutt1/Robo1 gene. Proc. Natl. Acad. Sci. USA 98:15062–15066.

↲ Yang L., Bashaw G. J. (2006) Son of sevenless directly links the Robo receptor to rac activation to control axon repulsion at the midline. Neuron 52:595–607.